The Electrochemistry of Porous Semiconductors

John J. Kelly and A.F. van Driel

1 Introduction

The porous semiconductor electrode provides an interesting example for the theme of this volume: electrochemistry at the nanoscale. In porous etching, the anodic reaction can be considered to occur at an array of "nanoelectrodes", the pore tips, while the remainder of the porous matrix remains electrochemically inactive. In this case, conditions are clearly different from those at a macroscopic surface. Porous electrodes can also exhibit another aspect, one in which charge transfer is not restricted to the pore fronts; instead, the whole internal surface of the matrix acts as an electrode with a very large area but with a reduced "thickness", corresponding to the dimensions of the pore wall. Such small dimensions, which can even lead to size quantization, play a critical role in the electrochemistry. In this chapter, we consider the factors that decide whether the electrochemical reaction occurs exclusively at the pore fronts or at the whole internal surface of the porous layer. We review the electrochemistry of the two cases and related chemical and physical properties. In addition, we compare some results of porous-etched single crystals with those of nanoporous electrodes made by deposition from colloidal suspension.

Porous solids are classified according to an IUPAC convention [1] which distinguishes three cases: "macroporous" refers to systems with pore diameters larger than 50 nm while "microporous" describes the range below 2 nm. The term "mesoporous" is used for the intermediate range. Since physical and chemical properties of these materials do not recognize sharp IUPAC definitions, we shall use a mixed notation: micro/mesoporous refers to microporous systems and mesoporous systems with dimensions bordering on microporous. Similarly, we use meso/macroporous to denote macroporous systems and larger-dimension mesoporous systems. One can also classify porous materials on the basis of the morphology. Pores may be

J.J. Kelly (✉)
Condensed Matter and Interfaces, Debye Institute, Utrecht University, P.O. Box 80000, 3508 TA, Utrecht, The Netherlands
e-mail: J.J.Kelly@phys.uu.nl

P. Schmuki, S. Virtanen (eds.), *Electrochemistry at the Nanoscale,* Nanostructure Science and Technology, DOI 10.1007/978-0-387-73582-5_6,

isotropic, that is, with a random orientation, or anisotropic when they follow electric current lines or preferred crystallographic orientations.

Since in the case of micro/mesoporous semiconductors the dimensions of the pore walls can be similar to the radius of the Bohr exciton, effects due to quantum confinement can be expected [2]. Porous silicon is the most spectacular of such systems. While bulk single-crystal silicon shows only a very weak photoluminescence in the near-infrared, porous silicon with pore-wall dimensions less than 10 nm gives a very strong emission in the visible spectral range. The emission shifts to the blue as the porous structures become smaller, that is, with stronger confinement. We can use this phenomenon as a diagnostic tool to give information about the exact location of electrochemical reactions.

The review, which deals with electrochemistry in aqueous solutions, is organized as follows. Chapter 2 deals with the charging of porous semiconductors, and the results are compared with those of conventional (nonporous) electrodes. Chapter 3 focuses on electrochemical reactions. There is a subdivision on the basis of the main type of charge carrier involved (majority, minority, or both). In each case, the process of porous etching is first considered (electrochemistry at the pore fronts), and this is followed by oxidation and reduction reactions (electrochemistry at the pore walls). In Chapter 4 we draw some general conclusions.

2 Charging of Porous Electrodes

In classical semiconductor electrochemistry, the reference point for the electrode is the flat-band potential, U_{fb} (Fig. 1(a)) [3]. At this potential, the surface and bulk concentrations of charge carriers are the same, and there is no electric field present in the semiconductor. If the applied potential U deviates from U_{fb}, then a space charge is created at the surface, as in a Schottky diode (Fig. 1(b,, c, and d). The concentration of majority carriers at the surface may increase (accumulation) or decrease (depletion). Under strong depletion, that is, for a large deviation from the flat-band condition, one may, in principle, observe inversion; the concentration of minority carriers at the surface is larger than that of the majority carriers. However, in aqueous systems, reactions of the minority carriers at the solid–solution interface generally prevents inversion; instead deep depletion is observed (see Section 2.2). In this section, we consider the charging of porous electrodes under conditions in which majority carriers are expected to accumulate (Section 2.1) or to be depleted (Section 2.2) at the surface of a macroscopic porous electrode. The morphology of the porous matrix plays an important role in determining the charging properties.

2.1 Accumulation

In the case of an n-type semiconductor, accumulation is achieved by making the potential of the electrode negative with respect to the flat-band potential ($U < U_{\mathrm{fb}}$),

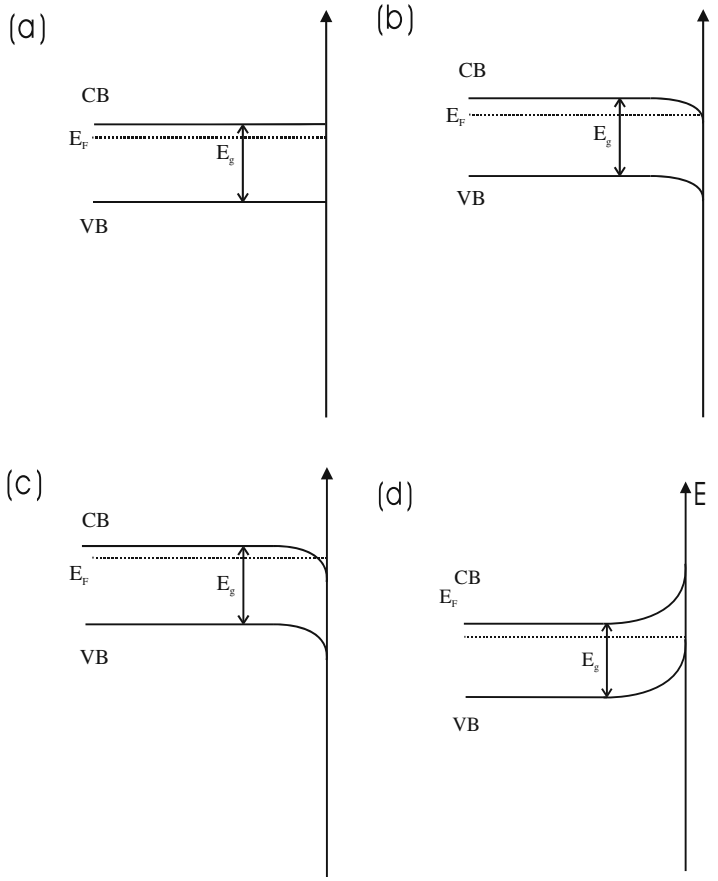

Fig. 1 Schematic band-energy diagram for an n-type semiconductor under flat-band conditions ($U = U_{fb}$) (**a**), accumulation conditions ($U < U_{fb}$) (**b**), under strong negative polarization (i.e., degeneracy, $U << U_{fb}$) (**c**), and depletion conditions ($U > U_{fb}$) (**d**). The conduction band (CB) and valence band (VB) are separated by the bandgap (E_g)

that is, by raising the Fermi level (see Fig. 1(b)). The majority carrier concentration at the surface becomes larger than that in the bulk. Eventually, the Fermi level passes through the conduction-band edge, and the surface becomes degenerate (quasi-metallic) (Fig. 1(c)). In this case, the Fermi level becomes pinned (the band edges at the interface become unpinned (Fig. 1(c)). The applied potential is now dropped across the Helmholtz layer in solution, as at a metal electrode. A corresponding situation holds for a p-type electrode at potentials positive with respect to the flat-band potential ($U > U_{fb}$) [3].

In contrast to the case of depletion (see Section 2.2), the space-charge layer capacitance for accumulation is large (in the case of degeneracy, comparable to the

capacitance of the Helmholtz layer at a metal electrode). Consequently, the space-charge layer has a thickness similar to that of the Helmholtz layer. In the case of a porous electrode, one would generally expect the accumulation layer to follow the contours of the internal surface area of the matrix, even for a microporous electrode. The interfacial capacitance should then be proportional to the *total* surface area. This was shown by Peter et al. [4] for n-type silicon during anodic porous etching in 40% HF/ethanol (1/1). The interfacial capacitance was determined by performing a potential sweep to negative potentials with a triangular voltage waveform at various stages in the etching process (Fig. 2(a)). The capacitance was shown to be linearly dependent on the anodic charge passed during etching (Fig. 2(b)) and independent of the current density used for forming the porous layer. By assuming a particular particle geometry (spherical, columnar), the authors were able to calculate typical particle dimensions from the surface area and the volume of silicon in the porous layer (inset Fig. 2(b)). During subsequent chemical dissolution of the porous matrix in the same electrolyte solution, the capacitance decreased with etching time, indicating a decrease in the particle dimensions. This pore broadening due to chemical etching gave rise to an intense photoluminescence, characteristic of porous silicon.

An equivalent charging experiment using cyclic voltammetry is not possible with p-type porous silicon in aqueous solution because of anodic oxidation of the semiconductor. In the n-type case, charging is not hindered by the Faraday reaction because hydrogen evolution has a large overpotential.

The charging curves in the work of Peter et al. [4] do not show the structure which might be expected from quantization effects (filling of discrete shells of quantized structures, electron–electron repulsion, etc.). This is probably due to the large degree of polydispersity in porous silicon. (Luminescence results described in the next section give strong indirect evidence for size quantization.) Striking quantization effects have been observed in porous solids deposited from colloidal suspensions of monodisperse nanoparticles or quantum dots, Fig. 3(a). An electrochemically gated transistor geometry was used to study porous layers formed in this way [5–7]. The insulating substrate was provided with two parallel gold tracks that acted as a source and drain. The electrode potentials of source and drain could be controlled by a potentiostat. A small potential difference between source and drain allowed measurement of the conductance of the layer. Under applied potential, the quantum dot layer equilibrates with the source/drain electrode by adjustment of the electron density in the layer; the charge injected is compensated by incorporation of additional positive ions into the pores of the film. By measuring the current (Fig. 3(a)) or the differential capacitance [5, 7] as a function of potential, the authors could follow the charging of the quantum dots. For both systems studied (ZnO particles with diameters in the 3–6 nm range [5] and CdSe particles with similar dimensions [6, 7]), a stepped charging is observed, which could be attributed to a sequential filling of the S and P orbitals of the quantum dots (Fig. 3(b)). The sequential filling of the discrete levels led to dramatic changes in the conductance of the films (Fig. 3(b)) and in the carrier mobility [5–7]. This provides further evidence for size quantization.

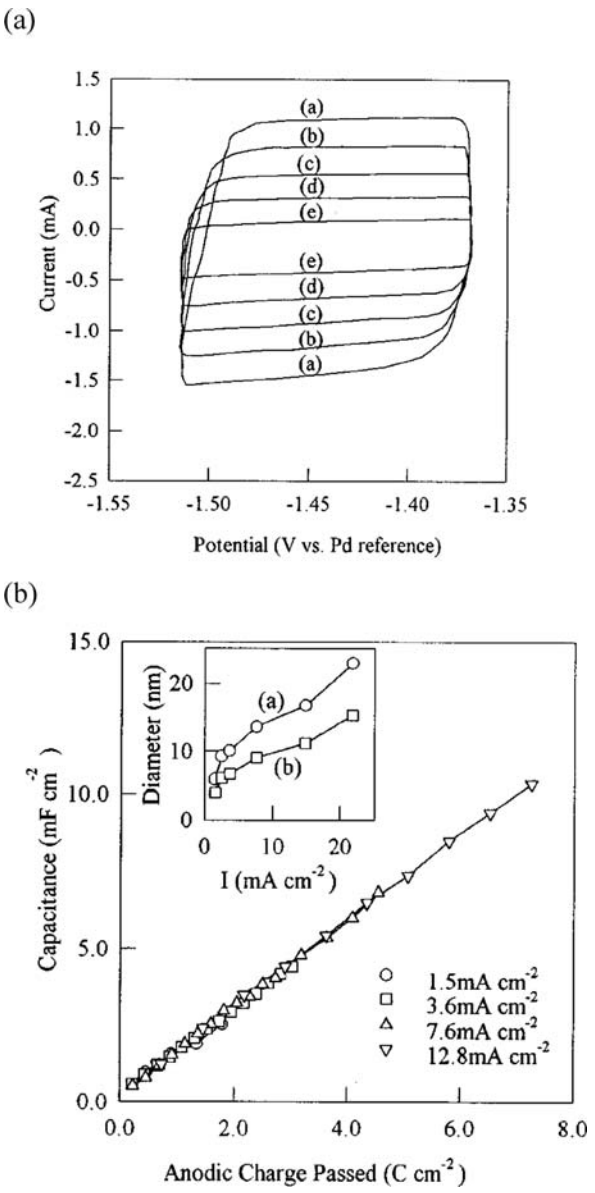

Fig. 2 (**a**) Cyclic voltammograms of n-type porous silicon in 40% HF. The sample was prepared by anodization at 14.8 mA cm^{-2} for 4 min to form a 6.8-μm thick porous layer. The scan rates were 250 (**a**), 200 (**b**), 150 (**c**), 100 (**d**), and 50 (**e**) mVs^{-1}. In (**b**) the interfacial capacitance is shown as a function of the anodic charge passed during formation of the porous layer. The current densities employed during porous etching are indicated in the figure. The inset shows the calculated average diameter as a function of the anodization current density for both a spherical (**a**) and columnar (**b**) geometry. Reprinted with permission from L.M. Peter, D.J. Riley, R.I. Wielgosz, "In situ monitoring of internal surface are during the growth of porous silicon", Applied Physics Letters, Vol. 66, p. 2355 (1995). Copyright (1995), American Institute of Physics

2.2 Depletion

Depletion occurs for an n-type semiconductor polarized positive with respect to the flat-band potential ($U > U_{fb}$, see Fig. 3(d)) and for a p-type semiconductor negatively polarized ($U < U_{fb}$) [3]. The thickness of the space-charge layer d_{sc} of a flat Schottky diode under depletion conditions is given by [8]:

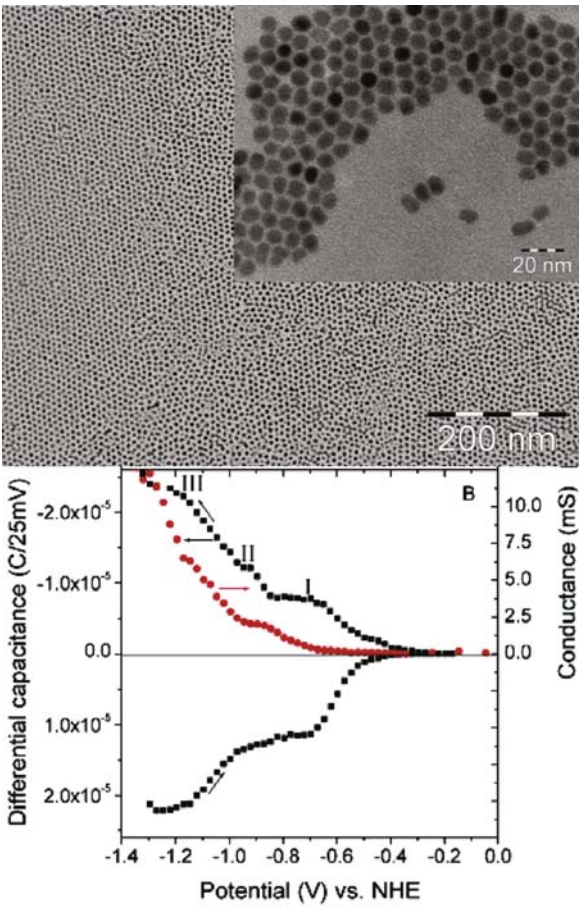

Fig. 3 (*top*) TEM image of 6.2-nm CdSe nanoparticles. The inset shows a magnified image of a monolayer of 8.4-nm CdSe nanoparticles. (*bottom*) Differential capacitance (solid squares) and long-range electronic conduction (open triangles) of 6.4-nm CdSe nanoparticle assemblies under steady-state conditions. Wave I in the charging curve occurs before the onset of electronic conduction; it is attributed to electron injection into localized states in the bandgap. Waves (II) and (III) are due to electron injection into quantized states of the nanoparticles. Reprinted with permission from A.J. Houtepen, D. Vanmaekelbergh, J. Phys. Chem. B, Vol. 109, p. 19634 (2005). Copyright (2005). American Chemical Society

$$d_{\mathrm{sc}} = \sqrt{\frac{2\varepsilon\varepsilon_0}{eN_{\mathrm{D}}}U_{\mathrm{sc}}} \tag{1}$$

where ε is the dielectric constant, ε_0 the permittivity of free space, U_{sc} the band bending (U-U_{fb}), e the electronic charge, and N_{D} the donor density. For a typical band bending of 1 eV, d_{sc} can vary between 11 and 332 nm for dopant densities in the range 10^{16}–10^{19} cm^{-3} ($\varepsilon = 10$). Although the space-charge layer will be somewhat different at the surface of a cylindrical pore or a hemispherical pore front, it is clear that the range of values of d_{sc} covers the range of pore and pore-wall dimensions on going from low mesoporous to macroporous. Consequently, the potential distribution is more complicated than in the case of degeneracy, resulting from strong accumulation. We can distinguish a number of cases which depend on the relative thickness of the space-charge layer (d_{sc}) and the pore-wall thickness (W).

(i) Micro/mesoporous electrodes ($d_{sc} > W$)
In this case, the typical dimensions of the porous layer are considerably smaller than d_{sc}, and the whole porous structure will be depleted, even for moderate values of U_{sc} [9]. The depletion layer is located at the interface between the porous layer and the (nonporous) substrate.

The absence of a space charge in the porous matrix is responsible for a somewhat unexpected dependence of the photoluminescence of micro/mesoporous silicon on applied potential. While the presence of a depletion layer in a conventional semiconductor electrode suppresses light emission (the electric field separates the electrons and holes before they can recombine), electrons and holes generated in a "field-free" porous structure are not spatially separated. Radiative recombination within quantized structures gives photoluminescence in the n-type silicon which persists to potentials strongly positive with respect to the U_{fb} value of the nonporous semiconductor. We return to this result in Section 3.3.

(ii) Meso/macroporous ($d_{sc} < \frac{1}{2}W$)

When the pore-wall dimensions are larger than 2 d_{sc}, the space-charge layer can be accommodated within the porous structure, following the contours of the pores (Fig. 4(a)). The depletion-layer capacitance depends in this case on the porosity; it can be orders of magnitude larger than that of the corresponding geometric surface [9–14].

(iii) Meso/macroporous electrodes ($d_{sc} > \frac{1}{2}W$)

Since d_{sc} is directly proportional to the square root of the band bending ($U - U_{fb}$), the space-charge layer can, at higher potential, become thicker than the pore walls ($d_{sc} > \frac{1}{2}W$). In this case, the porous structure becomes fully depleted (as in case (i)) and the depletion-layer capacitance drops drastically; the depletion layer is again located at the porous/nonporous interface. A fairly abrupt transition to a fully depleted structure has been observed in different systems, for example, n-type GaP (see Fig. 5) [10, 11] and n-type SiC [12, 13].

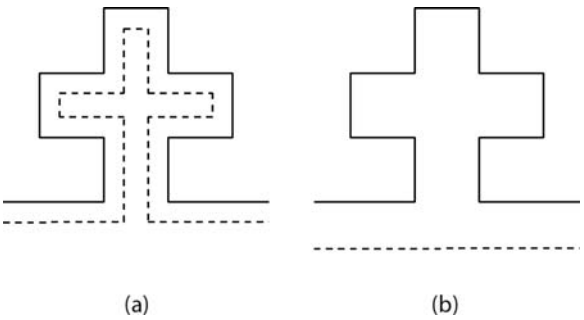

Fig. 4 Schematic representation of a porous structure under depletion conditions. In case (**a**) the depletion-layer width d_{sc} is smaller than half the wall thickness ($\frac{1}{2}$ W). The inner edge of the depletion layer follows the contours of the porous layer and the space-charge layer capacitance is very large. In case (**b**) the porous layer is completely depleted ($d_{sc} > \frac{1}{2}$ W). The depletion-layer edge is not located within the porous layer but at the interface between the porous layer and the substrate. In this case, the space-charge layer capacitance is similar to that of the flat electrode

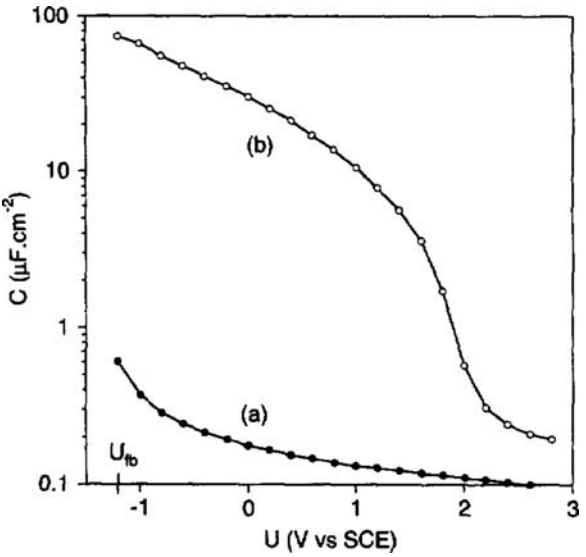

Fig. 5 The potential dependence of the space-charge layer capacitance of n-type GaP. Curve (**a**) refers to the nonporous electrode and curve (**b**) to the porous electrode. The etching charge passed in this case was about 5 C cm^{-2}. In case (**a**) the sharp drop in capacitance at higher potential corresponds to the transition from (**a**) to (**b**) in Fig. 4.The flat-band potential is denoted U_{fb}. Reprinted from Electrochimica Acta, J.J. Kelly and D. Vanmaekelbergh, "Charge carrier dynamics in nanoporous photoelectrodes", Vol. 43, p. 2773, Copyright (1998), with permission from Elsevier

3 Electrochemical Reactions

Reactions at semiconductor electrodes can be classified on the basis of the type of charge carrier involved in the interfacial process. Majority carrier reactions are expected when the surface concentration of holes in a p-type material or electrons in an n-type material is high, that is, in or close to accumulation conditions [3]. Minority carrier reactions can be initiated by injection from a species in solution. Alternatively, electron–hole pairs can be generated with supra-bandgap light. If the charge carriers are effectively separated by the electric field, that is, under depletion conditions, minority carrier reactions can be observed at the interface with solution. Finally, there is a third class of reaction in which recombination of electrons and holes determines the kinetics of the interfacial process; clearly, in this case, the surface concentration of both types of charge carrier is important.

In the context of this chapter, an important electrochemical reaction is the porous etching of the semiconductor. To dissolve a semiconductor valence band holes must be localized in surface bonds at the solution interface. Consequently, anodic etching of p-type electrodes having holes as majority carriers is expected to occur in the dark with an onset close to flat-band potential. To dissolve an n-type semiconductor, minority carriers must be provided. Generally, dissolution of the semiconductor is uniform with the whole surface etching at the same rate. Two factors distinguish porous

etching: (i) pores are initiated by localized attack at certain points on the surface and (ii) these pores are able to propagate. A third important process is pore branching which allows a three-dimensional matrix to be formed. There is a huge literature on the porous etching of semiconductors, and a wide range of models have been proposed to describe the various systems. Despite the rich variety of attempts to describe completely the mechanism of porous etching, no consensus has been achieved. The various models focus on specific aspects of porous etching, using their own language and their own level of description. These models have been reviewed by Chazalviel and co-workers [15], who classify them in terms of chemical models [16, 17], physical models [18, 19], and simulation approaches [20, 21]. In this chapter, we limit the discussion to certain "physical" models which reflect the theme of the volume: electrochemistry on the nanoscale. For an overview of porous etching of semiconductors, we refer the reader to review papers [15, 22, 23] and books [24–26].

In Section 3.1, we show how minority carriers can be generated and consider the role of minority carriers in pore formation and redox reactions at porous electrodes. Corresponding majority carrier reactions are considered in Section 3.2. In Section 3.3, reactions are described in which *both* electrons and holes are involved; such processes at micro/mesoporous electrodes give rise to interesting optical effects.

3.1 Minority-Carrier Reactions

There are three main approaches to generating minority carriers in a semiconductor electrode: by "injection" from a redox species in solution, by illumination with supra-bandgap light, and by band-to-band tunneling. Because the third approach is the most important mechanism for porous etching of a wide range of n-type semiconductors, we shall begin by discussing this case.

3.1.1 Electron Tunneling

It is generally accepted that the propagation of pores during anodic etching of n-type semiconductors in the dark is due to enhanced dissolution as a result of electron tunneling from the top of the valence band to the conduction band. This is made possible by the much higher electric field at the tip of the pores. This idea was first proposed by Theunissen [18] and extended by Beale [19] and others [27–29]. This model is able to account for much of the phenomena observed during porous etching of n-type semiconductors in the dark.

The electric field at the pore tip is described by an abrupt one-sided Schottky barrier [8]. During etching, a strong reverse bias is applied, inducing deep depletion at the surface of the semiconductor (Fig. 6). The thickness of the depletion (or space charge) region at a flat n-type semiconductor/electrolyte interface is given by Eq. (1). The electric field in the space-charge region, as shown in Fig. 6, has a maximum E_{max} at the semiconductor surface:

$$E_{max} = \frac{eN_D d_{sc}}{\varepsilon\varepsilon_0} \tag{2}$$

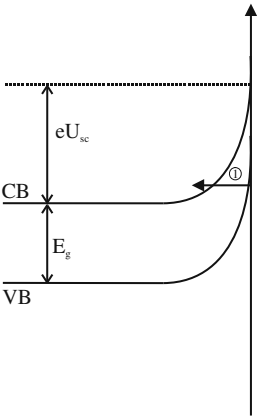

Fig. 6 Energy-band diagram for electron tunneling (step 1) under strongly anodic conditions (deep depletion). At the semiconductor–electrolyte interface, the electron tunnels from the valence band (VB) to the conduction band (CB). eU_{sc} is the potential difference with respect to flat-band conditions

where d_{sc} is the thickness of the space-charge layer. For GaP with a dopant density of 10^{17} cm^{-3} and an applied potential of 5 V with respect to the flat-band potential, the maximum field is 0.4×10^6 V cm^{-1}. As pointed out by several authors [19, 28, 29], the curvature of the pore tip leads to a local intensification of the electric field. As a consequence of the strong field, "breakdown" occurs selectively at the tip of the pore. Electrons tunnel from the top of the valence band to the conduction band (Fig. 6), thus providing holes at the surface needed for the dissolution of the solid. In the case of GaP in acidic solution, six holes are required for each formula unit of the semiconductor and the trivalent Ga and P products dissolve [10, 11, 25]

$$\mathrm{GaP} + 3\mathrm{H_2O} + 6\,\mathrm{h}^+ \rightarrow \mathrm{Ga(III)} + \mathrm{H_3PO_3} + 3\mathrm{H}^+ \tag{3}$$

Tunneling of electrons through the barrier and avalanche multiplication are well-known phenomena in strongly reverse-biased p–n junctions [8, 30]. The role of the dopant density in breakdown in p–n junctions has been studied extensively [30]. The breakdown voltage increases with decreasing carrier concentration. The same trend is observed for etching of GaP [31] and Si. Furthermore, the dopant density in a p–n junction must be high ($>5 \times 10^{17}$ cm^{-3}), in order to achieve the field required for tunneling [8]. This explains the observation that for porous etching (in the dark), only materials with a relatively high carrier concentration ($>10^{17}$ cm^{-3}) are used. Dark etching of lower-doped materials is not possible or results in nonuniform layers. As for low-doped p–n junctions, avalanche multiplication can occur in low-doped semiconductors, leading to strongly localized etch pits [19, 27, 31].

Two general trends could be observed in the potential dependence of etching of n-type single crystals (Si [27], GaP [31], and InP [32]): first, the pore diameter and the pore spacing both increase with increasing potential. This can be understood on the basis of the breakdown model. At low potential, the threshold field for breakdown is only reached if the radius of curvature is small, that is, only for small pores. Thus, a lower applied potential leads to the development of small pores. Second, the depletion layers around the pores cannot overlap. This is well demonstrated in GaP,

where initially all the pores grow isotropically from a point at the surface, while the pores subsequently "push" each other in a direction perpendicular to the surface [33]. A top view of a porous GaP layer (Fig. 7(a)) clearly shows that the pores are randomly distributed but do not overlap. This is related to the thickness of the depletion layer. At higher potential, the space-charge layer is larger (Eq. 1), which results in an increase of the spacing between the pores. A pore growing faster than the surrounding pores obtains more space and therefore a larger radius. A larger pore radius, however, means that the local electric field is weaker and thus the current density is reduced and thereby also the growth rate. This self-correcting mechanism explains the broadly observed flatness of the porous/nonporous interface.

The parallel between a p–n junction and an n-type semiconductor/solution junction under strong reverse bias is further demonstrated in the case of GaP by the observation of hot-carrier light emission [34]. Electroluminescence detected during porous etching of the semiconductor shows the same broad spectral features

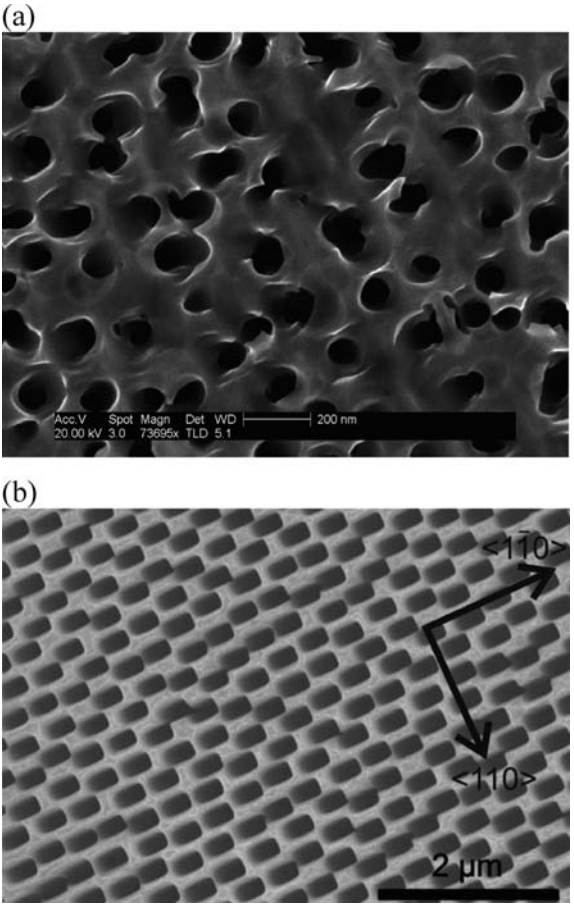

Fig. 7 Scanning electron microscopy picture of the top view of porous GaP. Sample (**a**) was etched at 10 V versus SCE in H_2SO_4 solution, and the pores are randomly oriented. Sample (**b**) was etched at 15 V versus SCE in HBr solution, and the pores have a rectangular shape and show self-organization. (**a**): Reprinted with permission from A.F. van Driel, B.P.J. Bret, D. Vanmaekelbergh, and J.J. Kelly, Applied Physics Letters, Vol. 84, p. 3852 (2004). Copyright (2004), American Institute of Physics. (**b**): Reproduced by permission of ECS – The Electrochemical Society, from J. Wloka, K. Mueller, and P. Schmuki, Electrochem. Solid State Lett. Vol. 8, p. B72 (2005)

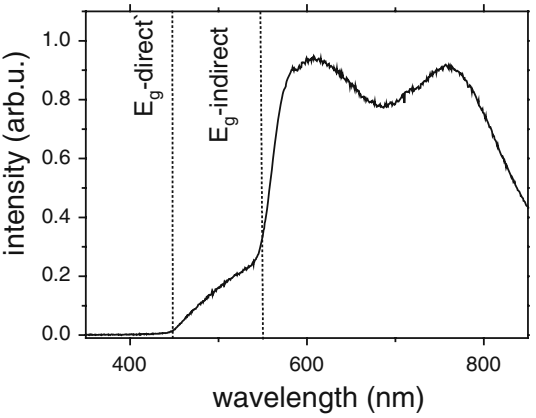

Fig. 8 Electroluminescence spectrum of n-type GaP during etching at 7 V in H_2SO_4 solution. The spectrum is very broad and contains a supra-bandgap contribution. The luminescence was attributed to a hot-carrier process. The direct and the indirect bandgaps are shown. Reprinted from Surface Science, A.F. van Driel, B.P.J. Bret, D. Vanmaekelbergh, and J.J. Kelly, "Hot carrier luminescence during porous etching of GaP under high electric field conditions", Vol. 529, p. 197, Copyright (2003), with permission from Elsevier

as those caused by reverse current flow in the p–n junction [30, 35], including a supra-bandgap contribution (Fig. 8). The electrochemical luminescence, which is generated at the tip of the pores, is related to the strong electric field in the depletion layer. After electron tunneling through the barrier, the electron is accelerated in the electric field. The electron can gain enough kinetic energy to excite a valence-band electron into the conduction band. The luminescence is attributed to the radiative recombination of these carriers. In contrast to the spatially uniform luminescence observed during porous etching of GaP, emission related to avalanche breakdown is strongly localized in bright spots [30]. The source of the luminescence, that is, the active etch front, moves during etching with a constant rate through the crystal. This allows one to measure in situ the wavelength-dependent transmittance of light of the porous layer [36].

In contrast to the random porous structure formed in GaP during etching in H_2SO_4 solution, strongly anisotropic, crystallographically oriented pores are formed during etching in HBr solution [37]. This was accompanied by strong electroluminescence [38], comparable to that observed during etching in H_2SO_4 solution [34]. In HBr solution, oscillations in the anodic current were accompanied by oscillations in light-emission intensity [38]. Current-line-oriented pores can also be grown in n-type InP [39–41]. By modulating the potential or the current density, various groups have grown modulated porous multilayers [33, 42].

3.1.2 Photogeneration

Illumination with supra-bandgap light can generate electrons and holes in a semiconductor electrode. Under depletion conditions, the charge carriers are separated; minority carriers are collected at the solid/solution interface where they can

participate in oxidation or reductions reactions, depending on the semiconductor type. On the other hand, under accumulation conditions or if the electric field of the depletion layer is weak, then the electrons and holes are not spatially separated, but recombine. In a direct-bandgap semiconductor, this can lead to light emission (photoluminescence). In this section, both aspects of photogeneration, reaction and recombination, are dealt with. "Reaction" includes photoanodic porous etching of n-type Si and passivation of the porous semiconductor. We also consider the effect of porous morphology on the quantum efficiency of photoanodic processes and on minority-carrier transport in porous semiconductors. Under "recombination", we show how the porous structure can change the kinetics of electron–hole recombination and thus influence the physical and chemical properties.

(i) Reaction

Under illumination, n-type semiconductors can be anodically dissolved at potentials much less negative than those required for breakdown (see Section 3.1.1.). If the electric field of the depletion layer is sufficiently strong to separate effectively photogenerated electrons and holes, then the holes reach the surface and cause oxidation and dissolution of the solid. In most cases, etching of the surface is uniform. Silicon in HF solution is exceptional in a number of respects. At lower-light intensity, the anodic photocurrent–potential curve (Fig. 9(b), lower curve) resembles that of other n-type semiconductors. At negative potential, no photocurrent is observed because of electron–hole recombination. Photocurrent onset results from the increasing electric field of the depletion layer. The current finally levels off. The limiting photocurrent, however, does not show a simple linear dependence on photon density. At very low light intensity, a quantum efficiency of 4 is observed, that is, one photon is responsible for the passage of four charge carriers in the external circuit. To explain this, we must assume that the photogenerated holes create oxidation intermediates that lead to injection of three electrons into the conduction band. As the light intensity is increased, the quantum efficiency drops to 2 and hydrogen

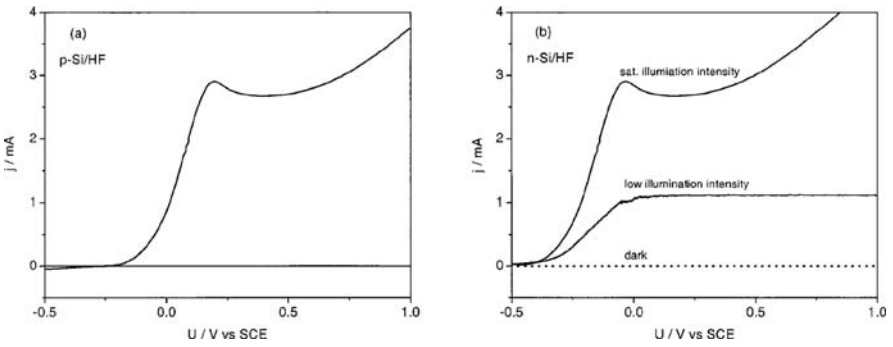

Fig. 9 Current–potential curves of (100) silicon in 1% HF solution at room temperature. Curve (**a**) is for p-type Si in the dark and (**b**) for n-type Si in the dark, at low light intensity and under saturated illumination conditions. A standard three-electrode electrochemical cell was used, the potential of the Si working electrode was varied with respect to that of a SCE reference with a scan rate of 20 mV/s. Reproduced with permission from Wiley, from Reference [25]

is evolved. The latter results from a chemical reaction between an intermediate and H^+ or HF. The total reaction can be represented in a simplified form by [16, 43]:

$$Si + 6HF + h^+ \rightarrow SiF_6^{2-} + H_2 + 4H^+ + e^- \quad (4)$$

Silicon dissolves as a hexafluoride species, and the silicon surface is hydrogen terminated under these conditions. At high light intensity, the photocurrent–potential curve becomes independent of the photon flux (Fig. 9(b), upper curve). A peak in the curve indicates the formation of oxide on the electrode. This is a four-hole reaction.

$$Si + 2H_2O + 4\,h^+ \rightarrow SiO_2 + 4H^+ \quad (5)$$

The oxide is soluble in HF solution, and dissolution is mass-transport controlled. At potentials approaching the peak potential, hydride termination is replaced by hydroxide or oxide termination. Beyond the peak potential, illuminated silicon is electropolished.

The most striking feature of the electrochemistry of n-type silicon illuminated in HF solution is the porosity produced by anodic etching. This result, first reported by Uhlir in 1956 [44], is not found with most other semiconductors. At low photocurrent densities, a random array of micro/mesopores is formed (this material is luminescent in the visible), while at higher current densities corresponding to potentials approaching the electropolishing range, the pores become wider (meso/macro) and tend to be anisotropic. Anisotropic-pore growth is very likely due to field-enhanced collection of minority carriers at the pore tips.

In a series of papers starting in 1990, Lehmann and co-workers [45–47] described very elegant work on macropore formation in silicon. Highly anisotropic pores could be formed by photoanodic etching of n-type (100) silicon whose surface had first been provided with etch pits, for example, by dark etching at high potential. The wafers were illuminated from the backside. Holes diffuse from the backside selectively to tip of the pores and dissolve the semiconductor locally. In this way, a porous structure can develop that corresponds to the predefined pore pattern. In order to cross the complete semiconductor width, the hole-diffusion length must be large. The hole-diffusion length increases with decreasing dopant density, and therefore low-doped materials must be used. Pore widths ranged from 0.5 to 100 μm, while a pore depth of 200 μm could be readily achieved (Fig. 10(a) and (b)) [48]. By starting with an ordered array of pits, produced by anisotropic etching through a photolithographically masked pattern, a perfectly ordered two-dimensional array of pores could be produced. Such lattices are interesting for photonic applications. The orientation of the primary pores is crystallographically determined; they grow in the ⟨100⟩ direction. Lehmann described macropore formation in n-type silicon as a self-adjusting mechanism characterized by a specific current density at the pore tip. At this current density, dissolution changes from a charge-transfer-limited to a mass-transport-limited regime. Passivation of the pore walls is attributed to a depletion of the minority carriers.

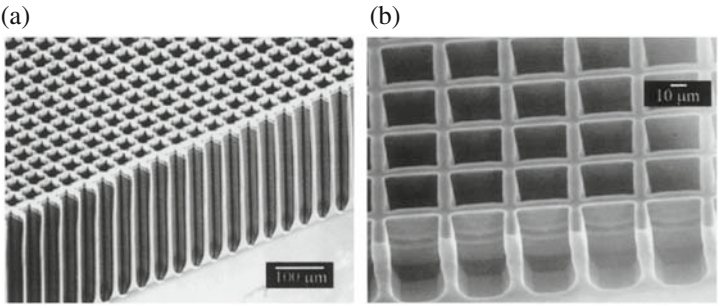

Fig. 10 (**a**) and (**b**) Scanning electron microscopy pictures of macropores formed in silicon. Etching was performed in 3% HF solution, starting with a predefined pore-pattern. The etching conditions allowed control of the pore wall thickness. Reprinted from Materials Science and Engineering B, P. Kleinmann, J. Linnros, and S. Petersson, "Formation of wide and deep pores in silicon by electrochemical etching", Vol. 69, p. 29, Copyright (2000), with permission from Elsevier

As pointed out by Lehmann, there are several limitations to the pore arrays that can be fabricated with n-type silicon [49]. Pores with a diameter down to 0.3 μm have been achieved. The lower limit is established by the diameter at which the intensification of the electric field is large enough to cause breakdown at the tip of the pore (see Section 3.1.1). There does not seem to be an upper limit for the pore radius. Pore widths up to 100 μm have been reported [48]. In principle, the pore spacing can be chosen arbitrarily. However, when the pore spacing is larger than twice the depletion-layer thickness ($W > 2d_{sc}$), the porous layer is not completely depleted. Holes can now diffuse between the pores and dissolve the pore walls. Usually low-doped materials are used for macropore formation in Si. This means that the depletion layer is wide (typically 1.5 μm for 10^{15} cm^{-3} doped n-type Si at 2 V) and for porous layers with a spacing smaller than $2d_{sc}$, the porous structure is depleted and thus protected against dissolution.

Föll and co-workers [50] extended earlier work of Lehmann by studying the dependence of macropore formation on the substrate orientation. Samples were cut from a large silicon crystal in various orientations between $\{100\}$ and $\{111\}$. The growth direction of the photoanodically formed macropores was found to be $\langle 100\rangle$ and $\langle 103\rangle$ with a switch over at a critical angle of 43°. Surprisingly, pores obtained by breakdown at high field without illumination always grow in the $\langle 100\rangle$ direction. The reason for such differences is not clear.

The shape of anisotropic macropores in n-type silicon can be tuned by means of the photocurrent density or the potential. Gösele and co-workers [51–53] have succeeded in making three-dimensional structures with a high degree of perfection by combined modulation of the applied potential and the light intensity (Fig. 11(a) and (b)). A subsequent anisotropic etching step could be used to extend the range of structures and to adjust the photonic properties of the system.

In HF-free acidic solution, porous n-type silicon passivates under illumination at positive potentials (depletion conditions) [54]. The oxide formed (see Eq. 5) is

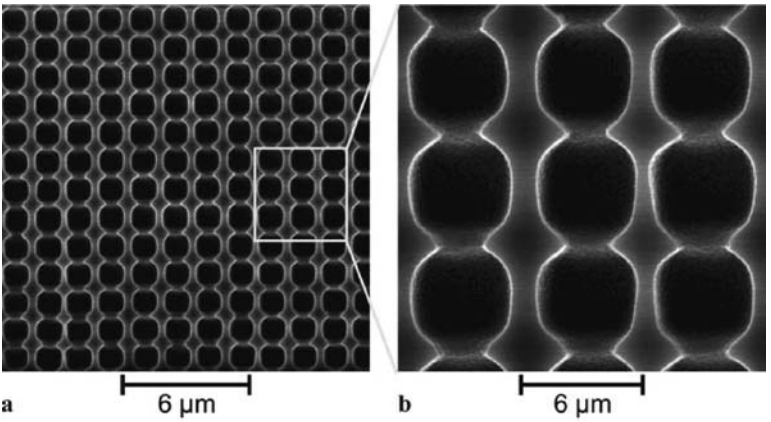

Fig. 11 Scanning electron microscopy pictures of strongly modulated porous n-type silicon samples. In (**a**) an overview is shown and in (**b**) the close-up. During porous etching of the Si crystal, the applied potential was modulated, resulting in a strongly modulated structure. Reproduced with permission by Springer, from S. Matthias, F. Muller, J. Schilling, and U. Gosele, Appl. Physics A, Vol. 80, p. 1391 (2005)

not soluble. In contrast to electrochemical oxide reactions in HF solution, oxidation occurs at the whole internal surface of the porous layer; this can be deduced from the charge involved in the oxidation reaction. Very likely, the pore fronts are passivated first, and this is followed by passivation of the pore walls. Photoanodic oxidation can be caused even by near-infrared light corresponding to the bandgap energy of the silicon substrate. Surprisingly, infrared-induced photoanodic oxidation of porous n-type silicon is accompanied by emission of visible light (electroluminescence). Infrared light cannot excite the wider bandgap porous semiconductor directly. Instead, holes generated under depletion conditions in the substrate must be injected into quantized structures of the porous matrix. This luminescence, which is closely connected to anodic oxidation, is also observed with porous p-type silicon. The mechanism will be discussed in Section 3.3.1.

The quantum efficiency of a photoelectrochemical reaction, that is, the number of charge carriers measured in the external circuit per absorbed photon, depends on (i) the efficiency with which the minority carriers are collected at the surface and (ii) the competition between surface recombination and the charge transfer reaction [12]. The collection efficiency depends on the penetration depth of the light $1/\alpha$ (where α is the absorption coefficient), the minority carrier diffusion length L_p (in the case of holes), and the thickness of the space-charge layer d_{sc}. For the simple case in which surface recombination can be disregarded, that is, all carriers reaching the surface are transferred to solution, the Gärtner model [9] for an illuminated Schottky diode can be used to calculate the quantum efficiency:

$$Q = j_p/\phi_o = 1 - \frac{e^{-\alpha d_{sc}}}{1 + \alpha L_p} \tag{6}$$

where j_p is the flux of holes to the surface and ϕ_o is the absorbed photon flux. The term on the right-hand side is the fraction of carriers lost to recombination in the semiconductor. For a direct-bandgap semiconductor, the absorption coefficient for energies above the bandgap is large and consequently the penetration depth of the light is small. In this case, minority carriers can be collected efficiently by migration ($1/\alpha < d_{sc}$) or by diffusion and migration ($1/\alpha < L_p$). In an indirect semiconductor, however, α above the bandgap is small and the penetration depth of the light may be very large ($1/\alpha > (d_{sc} + L_p)$). For example, in GaP (with a bandgap corresponding to 554 nm) illuminated with 514 nm light only about 1% of the photogenerated carriers reach the surface for a strong band bending of 1 eV. Consequently, the quantum efficiency is very low.

Porosity can affect the properties of photoelectrodes in two important ways [10–12, 25]. When the dimensions of the porous structures are comparable to the illumination wavelength, then the incident light is scattered and internally reflected within the porous layer. Equation (6) is no longer valid. The light is, in fact, absorbed much more effectively than in a nonporous medium, giving rise to a smaller effective penetration depth. In addition, light absorbed in a porous electrode generates minority carriers close to the solid/solution interface. The criterion for minority-carrier collection by the electrolyte is no longer $1/\alpha \leq (L_p + d_{sc})$ but $W/2 \leq (L_p + d_{sc})$. If this requirement is fulfilled, the minority carriers escape "bulk" recombination and reach the interface. The efficiency of reaction of minority carriers is then determined by competition between their transfer to solution and surface recombination. If the kinetics of the former process are efficient, then a high quantum yield can be obtained even for a light penetration depth which, in a nonporous electrode, would give a negligible yield.

There have been various reports of enhanced quantum efficiency due to porosity in photoelectrodes. Results obtained with n-type GaP are among the most spectacular. Curve (a) of Fig. 12 shows the photocurrent spectral response of a nonporous electrode. The quantum efficiency for photons with energy just above the fundamental absorption edge (2.24 eV) is low because, as already pointed out, the penetration depth $1/\alpha$ of the light is much larger than the retrieval length $d_{sc} + L_p$ of the minority carriers. As the photon energy is increased, $1/\alpha$ decreases (α increases), leading to an increase in efficiency. A strong increase is observed at 2.76 eV, which corresponds to the first direct optical transition in GaP. On the other hand, the quantum efficiency for the macroporous electrode (curve (b) in Fig. 12) reaches a value of 1 for photons of energy close to the fundamental absorption. Since the dimensions of the structural units are in the 100-nm range and the minority-carrier diffusion length is 50 nm, the criterion ensuring high efficiency $W/2 \leq (d_{sc} + L_p)$ is met for the potential range in which surface recombination is absent ($U_{sc} > 0.5$ V).

In addition to the efficient transfer of minority carriers across the semiconductor/solution interface, the majority carriers must be transported through the porous layer to the nonporous substrate and the back contact. Many recent experimental results show that electron transport through a mesoporous semiconducting network is a slow process due to carrier trapping. For instance, the average time that electrons need to travel through the system before collection, that is, the transit time, is

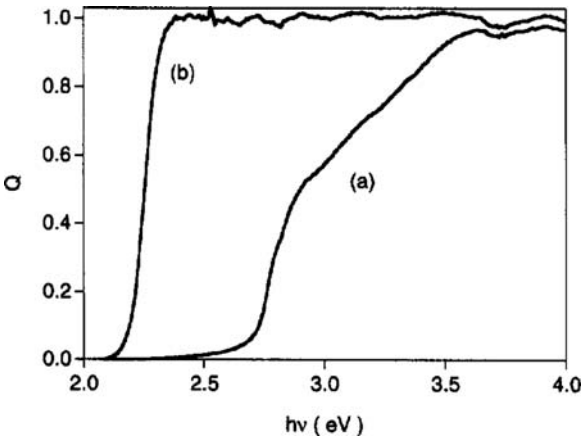

Fig. 12 The dependence of the photocurrent quantum efficiency (Q) on the photon energy (hν) for a polished n-type GaP electrode (**a**), and the same electrode after porous etching (**b**) [16 C cm^{-2}, 10 V vs. SCE]. The photocurrent, measured in 0.5 M H_2SO_4 solution at 1 V versus SCE, was due to anodic dissolution of the semiconductor. Reprinted from Electrochimica Acta, J.J. Kelly and D. Vanmaekelbergh, "Charge carrier dynamics in nanoporous photoelectrodes", Vol. 43, p. 2773, Copyright (1998), with permission from Elsevier

in the millisecond to second range [25]. As a result, photogenerated electrons can be lost before collection, by transfer to the oxidized species in the solution, a process characterized by a time constant τ_{rec}. Electron back transfer forms an important recombination process in the dye-sensitized photoelectrochemical solar cell based on the nanoparticle TiO_2 electrode [25].

(ii) Recombination

In a nonporous direct bandgap semiconductor, photogenerated electron–hole pairs recombining radiatively will give rise to photoluminescence. According to the Gärtner model (see Eq. 6), the PL intensity, I_{PL}, is given by

$$I_{PL} = \frac{\kappa \phi_0}{1 + \alpha L_p} e^{-\alpha d_{sc}} \tag{7}$$

where κ is the ratio of the rate of radiative recombination to the total recombination rate, that is, the photoluminescence quantum efficiency. The dependence of the depletion layer thickness d_{sc} on potential is given by Eq. (1). Figure 13 shows schematically the effect of applied potential on the emission intensity for an n-type semiconductor. Under depletion conditions at positive potential, the photogenerated electron–hole pairs are separated by the electric field preventing radiative recombination; instead, the flow of photocurrent (PC in Fig. 13) is favored. At potentials approaching U_{fb}, the surface concentration of majority carriers (holes in this case) increases and electron–hole recombination is favored. The photocurrent decreases with the onset of photoluminescence. Equation (6) predicts a limiting value of I_{PL} at $d_{sc} = 0$ ($I_{lim} = \kappa\phi_0/(1+\alpha L_p)$).

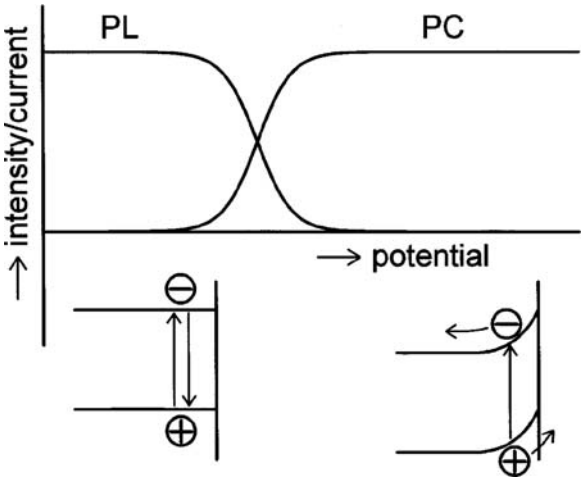

Fig. 13 Schematic representation of the potential dependence of the photocurrent (PC) and the photoluminescence intensity (PL) of an n-type semiconductor electrode in an indifferent electrolyte solution. Energy-band diagrams are shown for the illuminated semiconductor under flat-band (*left*) and depletion (*right*) conditions. Reprinted from Electrochimica Acta, J.J. Kelly, E.S. Kooij, and E.A. Meulenkamp, Vol. 45, p. 561, Copyright (1999), with permission from Elsevier

The potential dependence of the strong PL of micro/mesoporous silicon observed in indifferent electrolyte solution is, on the other hand, markedly different from that of a bulk electrode [55–57]. Under conditions corresponding to depletion in a non-porous electrode, potential-independent emission (PL) is observed (Fig. 14). Charge carriers generated within nanocrystallites are not spatially separated ($d_{sc} > W$) but

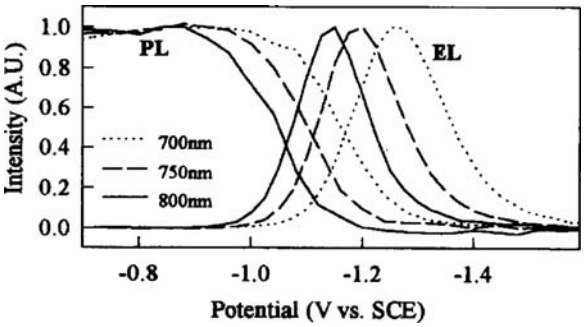

Fig. 14 Potential dependence of the electroluminescence (EL) and the photoluminescence intensity (PL) of a porous n-type Si electrode in an indifferent electrolyte solution (PL) and in $Na_2S_2O_8/H_2SO_4$ (EL) aqueous solution. Results are shown for three emission wavelengths. Note that the potential scale in this figure is reversed. Reprinted from J. Electroanalytical Chemistry, E.A. Meulenkmap, L.M. Peter, D.J. Riley, and R.I. Wielgosz, "On the mechanisms of the voltage tuning of photoluminescence and electroluminescence in porous silicon", Vol. 392, p. 97, Copyright (1995), with permission from Elsevier

recombine. The photoluminescence is quenched at potentials negative with respect to U_{fb}, a process that has been attributed to Auger recombination [57] or to hydrogen-mediated recombination [58]. The potential at which the PL intensity decreases depends on the wavelength of the emitted light: emission at lower energy (i.e., from larger crystallites) is quenched at more positive potentials than the high-energy emission (from the smallest crystallites). This has been attributed to a higher barrier for transfer of an electron from bulk silicon to small, more confined (wider bandgap) structures than to larger structures.

Interesting optical effects are observed during charging of the quantum-dot solids described in Section 2.1. The visible absorption spectrum of CdSe quantum dots in suspension shows characteristic sharp features that can be attributed to discrete excitonic transitions. These features are retained in the quantum-dot solid. As one would expect, such optical transitions are quenched when electrons are injected into the conduction levels at negative potentials. By studying the potential dependence of the absorption, Houtepen and Vanmaekelbergh [7] could conclude that the energy of the conduction S electrons is determined by the quantum confinement energy and by Coulomb repulsion between the S electron and all other electrons in the assembly. Wang et al. [59] observed photoluminescence from CdSe quantum-dot solids in the neutral, and the one- and two-electron charged states, even though the film is transparent at the emission wavelength. This striking result leads the authors to conclude that the threshold for amplified stimulated emission is strongly reduced, a result with important consequences for lasing. These two examples demonstrate the exciting perspectives of electrochemical gating in quantum-dot solid media.

3.1.3 Minority-Carrier Injection

Electrons can be extracted from the valence band of a semiconductor (i.e., holes can be "injected") if the acceptor levels of an oxidizing agent in solution correspond to the valence-band levels of the solid. This is the case for certain "simple" redox species such as Ce^{4+}, $IrCl_6^{2-}$, and $Fe(CN)_6^{3-}$ at Si [60]. For $Fe(CN)_6^{3-}$ in neutral aqueous solution, the reaction can be represented by

$$Fe(CN)_6^{3-} \rightarrow Fe(CN)_6^{4-} + h^+(VB) \tag{8}$$

In an n-type silicon electrode, holes held at the surface by the electric field of a depletion layer cause oxidation and passivation of the semiconductor. The oxide is not soluble in this case. Under accumulation conditions, the injected holes can recombine with conduction band electrons but, since radiative recombination in the indirect bandgap semiconductor is very inefficient, no light emission is observed.

Surprisingly, if holes are injected into n-type (or p-type) micro/mesoporous silicon at open-circuit potential, luminescence typical of the porous semiconductor is observed [60]. This emission, termed chemoluminescence, is related to oxidation of silicon (see Section 3.1.2), and its mechanism will be considered in Section 3.2.1. The fact that visible luminescence is observed shows that holes must be injected directly into quantized structures of the porous layer.

The presence of HF in a solution containing an oxidizing agent prevents passivation (see Eq. 4). Under such conditions, micro/mesoporous silicon can be formed at open-circuit potential. This process has been termed "stain etching", and the most widely used etchant contains HNO_3 as oxidizing agent [61, 62]. The mechanism involves two electrochemical reactions: reduction of the oxidizing agent to give holes (Eq. 8) which are used for oxidation of the semiconductor. Since porous etching occurs under open-circuit conditions, the rates of the two reactions must be equal. Stain etching has the advantage of being relatively simple (a counter electrode and voltage source are not required). However, the range of morphologies and thicknesses is rather limited. When "noble" metal ions are used as oxidizing agents, metal films with very distinct morphologies can be formed [63]. Galvanic exchange of gold on silicon gave, after surface modification of the metal with *n*-dodecanethiol, superhydrophobic surfaces with contact angles up to 165° [64].

Electrochemical oxidation of a reducing agent via the conduction band of a p-type semiconductor provides minority carriers (electrons) in the band. Such a reaction occurs with the methyl viologen radical cation $MV^{+\bullet}$ at silicon [65, 66]

$$MV^{+\bullet} \rightarrow MV^{2+} + e^{-}(CB) \tag{9}$$

The observation of visible luminescence during this reaction at porous p-type silicon under accumulation conditions indicates that electrons are injected into the porous matrix where they subsequently recombine with the majority carriers.

3.2 Majority-Carrier Reactions

3.2.1 p-Type Semiconductors

For most p-type semiconductors in indifferent electrolyte solution, oxidation of the solid is the main reaction involving majority carriers, that is, valence-band holes. (For wide-bandgap covalent semiconductors such as GaN and SiC, oxidation of water to oxygen may compete with oxidation of the semiconductor.) In the context of this chapter, the most interesting reaction is clearly the porous etching of silicon in HF solution. A typical current–potential curve is shown in Fig. 9(a). Initially the anodic oxidation current increases exponentially with increasing potential. Two holes are involved in the reaction, and a hydrogen molecule is formed via a chemical reaction of protons with reaction intermediates [67]. This process is clearly analogous to that observed with illuminated n-type Si at lower light intensity (see Eq. 4). Silicon dissolves as a hexafluoride complex.

$$Si + 6HF + 2h^{+} \rightarrow SiF_6^{2-} + 4H^{+} + H_2 \tag{10}$$

In this potential range, luminescent micro/mesoporous silicon is formed. At more positive potential, a maximum is observed in the current as for n-type Si at high light intensity, and the oxidation mechanism changes. An oxide layer is formed

(Eq. 5). Since the oxide is soluble in HF solution and the rate of dissolution is mass-transport controlled, electropolishing of the silicon surface is observed in the dark.

Macropores can also be grown in p-type Si [68]. This approach has the advantage that illumination is not required. The result is unexpected. To ensure sufficient holes at the surface, a forward bias is required. The pore walls are therefore not protected against dissolution ($d_{sc} < W$), as is the case for n-type Si. The mechanism is not well understood. The presence of surfactants [69] or the high resistivity of the substrate [70, 71] was proposed as key factors in the protection of the pore walls against dissolution. Both models are disputed [72, 73]. The complicating factor in the discussion is that etching is performed close to the flat-band potential; the exact electronic state is not known. Lehmann [72] proposed a mechanism in which it was assumed that the surface is slightly depleted of holes. Therefore, at the pore walls and pore tips, there is a diffusion current toward the surface. However, since the electrode is under slight reverse conditions, there is also a field current in the opposite direction. Under equilibrium conditions, both components compensate. When a positive potential is applied, the field current decreases, but the diffusion current remains constant. The diffusion current now determines etching and is larger at the tip of the pores. Geometrical factors are responsible for this. Because of this, a porous structure can develop. A stability analysis of macropore formation in p-type Si has been presented in Wehrspohn et al. [74].

In contrast to etching in HF solution for which the reaction occurs only at the pore fronts, in HF-free solution, anodic oxidation leads to passivation of the whole surface [54, 75–78]. This can be deduced from the charge required to achieve passivation, which is much higher for a porous electrode. Further evidence that the microporous layer is oxidized comes again from the observation of strong visible luminescence during the anodic reaction, typical of light emission from porous silicon (see Section 3.3.3).

Reducing agents whose donor levels correspond to the valence band of a semiconductor can compete for the surface holes and thus suppress or prevent anodic dissolution or passivation. Electrons may also be transferred from the reducing agent directly to electron-deficient surface bonds (the intermediates of the anodic dissolution process), thereby repairing the bonds and "stabilizing" the semiconductor [54]. It has been shown that the ferrocyanide ion can be oxidized at p-type porous silicon and, in this way, partially stabilize the semiconductor. As would be expected, this process quenches the luminescence. There is evidence to suggest that stabilization occurs via intermediates of the oxidation reaction.

3.2.2 n-Type Semiconductors

For an n-type semiconductor in an aqueous indifferent electrolyte solution, reduction of protons or of water to give hydrogen is the main reaction of the majority carriers. If the acceptor levels of a redox couple in solution overlap with the conduction-band levels of the solid, then the oxidized form can be reduced under accumulation conditions. In a porous semiconductor, this is likely to occur at the

whole internal surface of the electrode (see Section 2.1), if mass transport of electroactive species is not a problem. The rate of reduction depends on the electron concentration in the porous layer and thus increases as the electrode potential is made more negative. Two reactions of this type are interesting: electrodeposition of metal and reduction of strong two-electron oxidizing agents. The latter will be considered in Section 3.3.1.

It is possible to cover the whole interior surface of a porous semiconductor with a metal by cathodic reduction of metal ions via the conduction band. An example is gold electrodeposition from gold cyanide solution in macroporous n-type GaP [14]. A metal that forms a blocking contact with the semiconductor will give a Schottky diode with exceptional properties. The contact area of the diode is much larger than the geometric area. Minority carriers photogenerated in such a device can be collected with high efficiency when the dimensions of the pore walls are comparable to or smaller than the minority-carrier diffusion length (see Section 3.1.2).

3.3 Combined Majority/Minority-Carrier Processes

Injection of minority carriers into a semiconductor under accumulation conditions generally leads to recombination with the majority carriers. In that sense, the reactions described in Section 3.1.3 constitute an example of combined electron–hole processes. In this section, we consider some more complex hole- and electron-injecting reactions which, at porous electrodes, give interesting optical results (Sections 3.3.1 and 3.3.2, respectively).

3.3.1 Hole Injection

Reduction of a certain class of two-electron oxidizing agents, for example, the peroxydisulphate anion ($S_2O_8^{2-}$), known to give rise to "photocurrent doubling" at p-type semiconductors, can occur at n-type electrodes in the dark. The interesting feature of such reactions is that the first conduction band step

$$S_2O_8^{2-} + e^-(CB) \rightarrow SO_4^{2-} + SO_4^{-\bullet} \tag{11}$$

gives a strongly oxidizing species (in this case the radical anion $SO_4^{-\bullet}$) [55, 79, 80] which can inject a hole into the valence band of most semiconductors:

$$SO_4^{-\bullet} \rightarrow SO_4^{2-} + h^+(VB) \tag{12}$$

The injected holes can recombine with the majority electrons to provide electroluminescence. The observation of strong luminescence in the visible range, from micro/mesoporous n-type silicon, is clear evidence that holes are injected directly into quantized structures in the porous matrix.

The potential dependence of the spectral distribution of the electroluminescence (and of the photoluminescence) provides further evidence for quantization (see

Fig. 14) [56–58, 81]. Onset of luminescence is at a potential negative with respect to the onset potential for reduction of $S_2O_8^{2-}$. The emission passes through a maximum and is quenched at negative potential. Quenching is attributed to the same mechanisms as proposed for PL quenching. An interesting aspect of the emission from this system is its "voltage tunability"; the emission maximum shifts to shorter wavelength as the potential is made more negative. It has been suggested that this effect is also due to quantum confinement. Because of band-edge mismatch, supply of majority carriers to porous structures depends on their size. A more negative potential is required to supply the conduction band of smaller structures with electrons; these electrons are required for the first step of the $S_2O_8^{2-}$ reduction to trigger the subsequent hole-injection reaction. A similar voltage tuning is observed for PL (Fig. 14).

Peter and Wielgosz [82] produced electroluminescence in porous p-type silicon in peroxydisulphate solution by illuminating the substrate from the back side. The electrode was cathodically (reverse) biased. Electrons generated by light in the substrate accumulate in the porous layer, where they trigger the peroxydisulphate reduction. Voltage tuning of the emission was observed, similar to that found for porous n-type silicon in the dark.

3.3.2 Electron Injection

Under anodic polarization in HF-free neutral or acidic solution, p-type micro/mesoporous silicon is oxidized and passivates (Fig. 15(a)) [75–79] (see Section 3.2.1). During this process, visible light is emitted (Fig. 15(b)). This was, in fact, the first report of electroluminescence from porous silicon. The maximum in the emission peak shifts to shorter wavelength as oxidation progresses.

That a valence-band process involving holes is essential for inducing light emission could be confirmed by experiments in which n-type silicon, anodically (reverse) biased, was illuminated with infrared light that was absorbed by the substrate but not by the porous layer [54]. The photogenerated electrons and holes are spatially separated, and the electrons are collected at the back contact, giving photocurrent in the external circuit. Under influence of the electric field of the depletion layer at the interface of porous and nonporous regions, the holes accumulate at the substrate/porous silicon interface. On injection into the porous matrix, the holes cause oxidation and, ultimately, passivation of the solid.

For luminescence to occur, conduction-band electrons are also required. Under the conditions of this experiment (reverse bias), the majority carriers are depleted in the porous layer. As described in Section 3.1.2, there is strong evidence to show that intermediates of the anodic oxidation reaction of silicon have energy levels quite high in the bandgap of the semiconductor. Electrons thermally excited from such states into the conduction can recombine radiatively with valence-band holes. A similar anodic electroluminescence was observed for p-type, single-crystal InP in HCl solution [83]. The silicon process can be represented by the schematic reactions.

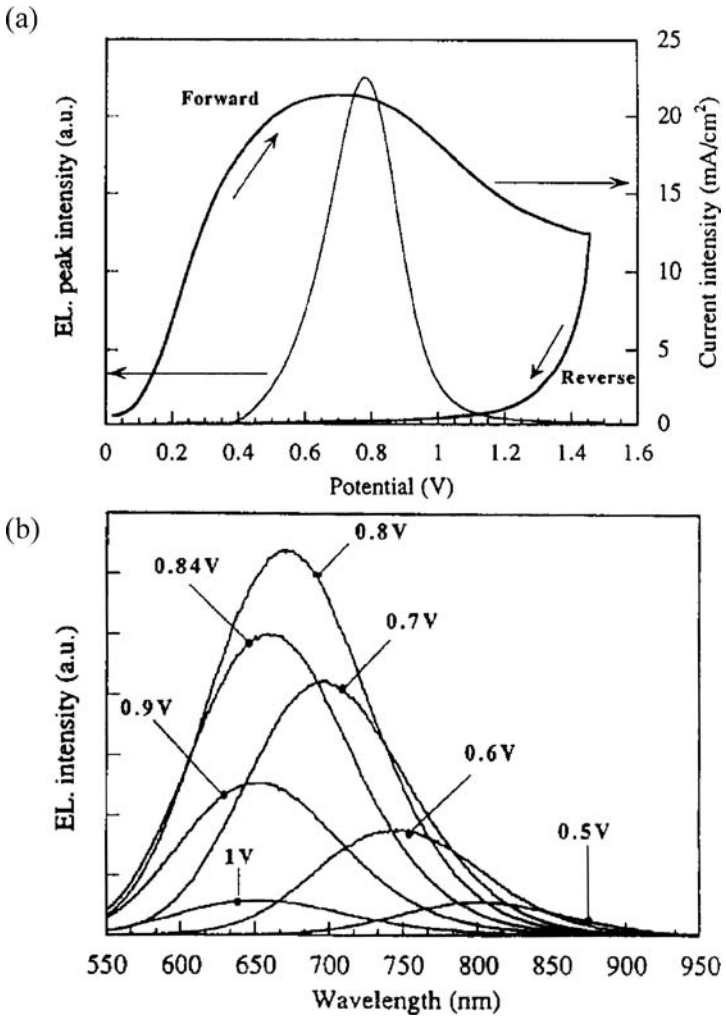

Fig. 15 (**a**) Anodic current density (*right* axis) and electroluminescence (EL) peak intensity (*left* axis) of p-type porous Si in 1 M H_2SO_4 solution, as a function of applied potential versus SCE. Both forward and reverse scans are shown; no EL was observed during the reverse scan. (**b**) The EL spectral evolution during a scan of the potential from 0 V to 1.2 V. Reprinted from Thin Solid Films, S. Billat, F. Gaspard, R. Herino, M. Ligeon, F. Muller, F. Romestain, and J.C. Vial, "Electroluminescence of heavily doped p-type porous silicon under electrochemical oxidation in the potentiostatic regime", Vol. 263, p. 239, Copyright (1995), with permission from Elsevier

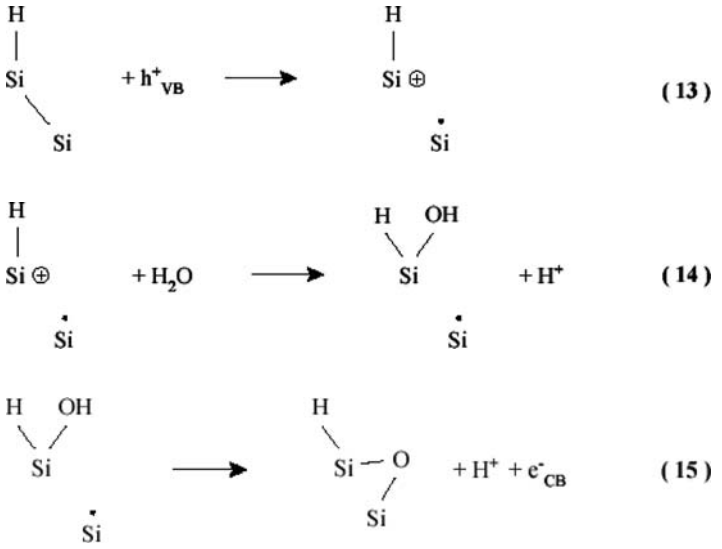

The blue shift in the visible emission observed during oxidation of both p-type silicon in the dark and n-type silicon under infrared illumination can be explained by size-selective hole injection. The porous layer contains nanostructures (crystallites) with a broad distribution of sizes. The energy barrier for hole transfer from the substrate to quantized structures is smallest for the largest crystallites; the effective bandgap is close to that of bulk silicon (the mismatch of the valence-band edges is small). Such regions of the porous layer will be oxidized first giving longer wavelength emission. As oxidation progresses, these regions become passivated and holes are injected into smaller crystallites, more confined structures. This results in a shift of the emission to shorter wavelengths. Eventually, the luminescence is quenched when the porous matrix is completely passivated.

It is, perhaps, not surprising that the presence of the reducing agent $Fe(CN)_6^{4-}$ in solution quenches the luminescence. As reported in Section 3.2.1, $Fe(CN)_6^{4-}$ can suppress oxidation of silicon by electron injection, very likely into intermediates of the oxidation reactions, for example:

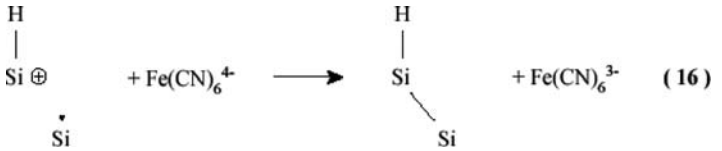

thereby "repairing" the electron-deficient bond (this reaction competes with injection of electrons into the conduction band, which is essential for light emission). A similar role is played by the Fe^{2+} ion in suppressing the anodic electroluminescence of p-type InP.

Instead of being supplied from the substrate, as described above, holes can also be injected directly into the porous matrix from an oxidizing agent in solution at open-circuit potential (Sections 3.1.3 and 3.2.1). This, of course, causes passivation in fluoride-free solution. Here again, luminescence is observed, but at open-circuit potential. The emission mechanism is, however, very likely the same as that described above for anodic luminescence.

4 Conclusion

The electrochemical reactions that occur at the internal surface of a porous electrode resemble those observed at macroscopic electrodes. A number of examples are described in this review. The potential dependence of the reaction rate may differ somewhat in the two cases. In confined systems, a larger "overpotential" may be required to drive the reaction. This is caused by the energy barrier at the interface between the smaller bandgap substrate and quantized regions in the micro/mesoporous layer and is a consequence of mismatch of valence- and conduction-band edges. The fact that the electrochemical reaction can occur at both the pore fronts (bulk electrode) and within the porous layer may complicate the analysis of the kinetics of electrochemical reactions. The porosity of the electrode has been shown to give rise to striking effects: strongly potential-dependent space-charge capacitances, unexpectedly high quantum efficiencies for photoelectrochemical reactions, quantized conduction due to charge injection, and characteristic light emission, which is not observed for nonporous electrodes.

Different questions are encountered in the electrochemistry of pore formation. It is, perhaps, not surprising that meso- and macropores nucleate at crystallographic defects at the semiconductor surface. The work of the groups of Lehmann and Gösele has shown that etch-pit patterns, produced photolithographically, can serve to fabricate impressive two- and three-dimensional meso/macroporous structures. The mechanism of nucleation of micro/mesopores is still unclear. Morphological stability models proposed for low-Ohmic p-type and (illuminated) n-type Si give insight into the initial stages of surface development. A kinetic model based on chemical and electrochemical steps is also interesting in this respect, but needs to be further elaborated. Propagation of pores requires localized dissolution at the pore fronts; this means that the pore walls must remain immune. When etching is carried out under depletion conditions, as in photoetching of meso/macropores in n-type Si (Section 3.1.2) or etching of n-type semiconductors in the dark under breakdown conditions (Section 3.1.1), then overlap of adjacent space-charge layers and majority-carrier depletion can explain the stability of the pore walls. In the case of compound semiconductors differences in the reactivity of the different crystal planes may be important, with pore propagation in "easy" crystallographic directions giving rise to facetted pore walls. Pore propagation in micro/mesoporous Si (n-type and p-type) is not well understood. Surface hydride very likely plays a role in pore-wall passivation. Quantum-size effects may be important for the electrochemistry at

structures with dimensions under 10 nm. One of the most intriguing questions in the field of porous semiconductors is the reason why Si in HF solution is so different in many respects from other semiconductors.

The relevance of porous semiconductors is clearly attested by the successful series of conferences "Porous Semiconductors: Science and Technology" which have been held biannually since 1998. (The last meeting was in Sitges, Spain, in March 2006.) The proceedings of these meetings [85, 86] give an overview of the wide range of basic science and applications involved. Electrochemistry continues to play an essential role in this field.

References

1. T. J. Barton, L. M. Bull, W. G. Klemperer, D. A. Loy, B. McEnaney, M. Misono, P. A. Monson, G. Pez, G. W. Scherer, J. C. Vartuli, and O. M. Yaghi, Chem. Mat., **11**, 2633 (1999).
2. A. G. Cullis, L. T. Canham, and P. D. J. Calcott, J. Appl. Phys., **82**, 909 (1997).
3. S. R. Morrison, Electrochemistry at Semiconductor and Oxidized Metal Electrodes, Plenum Press, New York, (1980).
4. L. M. Peter, D. J. Riley, and R. I. Wielgosz, Appl. Phys. Lett., **66**, 2355 (1995).
5. A. L. Roest, J. J. Kelly, D. Vanmaekelbergh, and E. A. Meulenkamp, Phys. Rev. Lett, **89**, 036801 (2002).
6. D. Yu, C. J. Wang, and P. Guyot-Sionnest, Science, **300**, 1277 (2003).
7. A. J. Houtepen and D. Vanmaekelbergh, J. Phys. Chem. B, **109**, 19634 (2005).
8. S. M. Sze, Semiconductor Devices: Physics and Technology, 2nd ed., Wiley, New York, (1981).
9. J. J. Kelly and D. Vanmaekelbergh, Electrochim. Acta, **43**, 2773 (1998).
10. B. H. Erné, D. Vanmaekelbergh, and J. J. Kelly, Adv. Mater., **7**, 739 (1995).
11. B. H. Erné, D. Vanmaekelbergh, and J. J. Kelly, J. Electrochem. Soc., **143**, 305 (1996).
12. J. van de Lagemaat, M. Plakman, D. Vanmaekelbergh, and J. J. Kelly, Appl. Phys. Lett., **69**, 2246 (1996).
13. A. O. Konstantinov, C. I. Harris, and E. Janzen, Appl. Phys. Lett., **65**, 2699 (1994).
14. D. Vanmaekelbergh, A. Koster, and F. I. Marin, Adv. Mater., **9**, 575 (1997).
15. J. N. Chazalviel, R. B. Wehrspohn, and F. Ozanam, Mater. Sci. Eng. B-Solid State Mater. Adv. Technol., **69**, 1 (2000).
16. E. S. Kooij and D. Vanmaekelbergh, J. Electrochem. Soc., **144**, 1296 (1997).
17. H. Foll, M. Christophersen, J. Carstensen, and G. Hasse, Materials Science & Engineering, **39**, 93 (2002).
18. M. J. J. Theunissen, J. Electrochem. Soc., **119**, 351 (1972).
19. M. I. J. Beale, J. D. Benjamin, M. J. Uren, N. G. Chew, and A. G. Cullis, J. Cryst. Growth, **73**, 622 (1985).
20. R. L. Smith and S. D. Collins, J. Appl. Phys., **71**, R1 (1992).
21. Y. Kang and J. Jorne, J. Electrochem. Soc., **140**, 2258 (1993).
22. H. Foll, S. Langa, J. Carstensen, M. Christophersen, and I. M. Tiginyanu, Adv. Mater., **15**, 183 (2003).
23. X. G. Zhang, J. Electrochem. Soc., **151**, C69 (2004).
24. V. Lehmann, Electrochemistry of Silicon; instrumantation, science, materials and applications, Wiley-VCH, Weinheim, (2002).
25. J. J. Kelly and D. Vanmaekelbergh, Porous etched semiconductors; formation and characterization, Chapter 4 of *The electrochemistry of nanomaterials*, Wiley-VCH, Weinheim (Germany), (2001).

26. X. G. Zhang, Electrochemistry of silicon and its oxide, Kluwer Academic/Plenum Publishers, Dordrecht, (2001).
27. V. Lehmann, R. Stengl, and A. Luigart, Mater. Sci. Eng. B-Solid State Mater. Adv. Technol., **69**, 11 (2000).
28. P. C. Searson, J. M. Macaulay, and F. M. Ross, J. Appl. Phys., **72**, 253 (1992).
29. X. G. Zhang, J. Electrochem. Soc., **138**, 3750 (1991).
30. S. Mahadevan, S. M. Hardas, and G. Suryan, Phys. Status Solidi A, **8**, 335 (1971).
31. J. Gómez Rivas, A. Lagendijk, R. W. Tjerkstra, D. Vanmaekelbergh, and J. J. Kelly, Appl. Phys. Lett., **80**, 4498 (2002).
32. A. Hamamatsu, C. Kaneshiro, H. Fujikura, and H. Hasegawa, J. Electroanal. Chem., **473**, 223 (1999).
33. R. W. Tjerkstra, J. Gómez Rivas, D. Vanmaekelbergh, and J. J. Kelly, Electrochem. Solid State Lett., **5**, G32 (2002).
34. A. F. van Driel, B. P. J. Bret, D. Vanmaekelbergh, and J. J. Kelly, Surf. Sci., **529**, 197 (2003).
35. M. Gershenzon and R. M. Mikulyak, J. Appl. Phys., **32**, 1338 (1961).
36. A. F. van Driel, D. Vanmaekelbergh, and J. J. Kelly, Appl. Phys. Lett., **84**, 3852 (2004).
37. J. Wloka, K. Mueller, and P. Schmuki, Electrochem. Solid State Lett., **8**, B72 (2005).
38. J. Wloka, D. J. Lockwood, and P. Schmuki, Chem. Phys. Lett., **414**, 47 (2005).
39. T. Takizawa, S. Arai, and M. Nakahara, Jpn. J. Appl. Phys. Part 2 – Lett., **33**, L643 (1994).
40. S. Langa, I. M. Tiginyanu, J. Carstensen, M. Christophersen, and H. Foll, Appl. Phys. Lett., **82**, 278 (2003).
41. S. Langa, I. M. Tiginyanu, J. Carstensen, M. Christophersen, and H. Foll, Electrochem. Solid State Lett., **3**, 514 (2000).
42. S. Langa, M. Christophersen, J. Carstensen, I. M. Tiginyanu, and H. Foll, Phys. Status Solidi A-Appl. Res., **197**, 77 (2003).
43. H. J. Lewerenz, J. Stumper, and L. M. Peter, Phys Rev Lett, **61**, 1989 (1988).
44. A. Uhlir, Bell Syst. Technol., **35**, 333 (1956).
45. V. Lehmann, J. Electrochem. Soc., **140**, 2836 (1993).
46. V. Lehmann and H. Foll, J. Electrochem. Soc., **137**, 653 (1990).
47. S. Ottow, V. Lehmann, and H. Foll, J. Electrochem. Soc., **143**, 385 (1996).
48. P. Kleimann, J. Linnros, and S. Petersson, Mater. Sci. Eng. B-Solid State Mater. Adv. Technol., **69**, 29 (2000).
49. V. Lehmann and U. Gruning, Thin Solid Films, **297**, 13 (1997).
50. S. Ronnebeck, J. Carstensen, S. Ottow, and H. Foll, Electrochem. Solid State Lett., **2**, 126 (1999).
51. S. Matthias, F. Muller, C. Jamois, R. B. Wehrspohn, and U. Goesele, Adv. Mater., **16**, 2166 (2004).
52. S. Matthias, F. Muller, and U. Goesele, J. Appl. Phys., **98**, 023524 (2005).
53. S. Matthias, F. Muller, J. Schilling, and U. Goesele, Appl. Phys. a-Mater, **80**, 1391 (2005).
54. E. S. Kooij, A. R. Rama, and J. J. Kelly, Surf. Sci., **370**, 125 (1997).
55. L. T. Canham, W. Y. Leong, M. I. J. Beale, T. I. Cox, and L. Taylor, Appl. Phys. Lett., **61**, 2563 (1992).
56. L. M. Peter, D. J. Riley, R. I. Wielgosz, P. A. Snow, R. V. Penty, I. H. White, and E. A. Meulenkamp, Thin Solid Films, **276**, 123 (1996).
57. L. M. Peter, D. J. Riley, and P. A. Snow, Electrochem. Commun., **2**, 461 (2000).
58. J. J. Kelly, E. S. Kooij, and D. Vanmaekelbergh, Langmuir, **15**, 3666 (1999).
59. C. J. Wang, B. L. Wehrenberg, C. Y. Woo, and P. Guyot-Sionnest, J. Phys. Chem. B, **108**, 9027 (2004).
60. E. S. Kooij, K. Butter, and J. J. Kelly, J. Electrochem. Soc., **145**, 1232 (1998).
61. D. Mills, M. Nahidi, and K. W. Kolasinski, Physica Status Solidi A, **202**, 1422 (2005).
62. E. Vazsonyi, E. Szilagyi, P. Petrik, Z. E. Horvath, T. Lohner, M. Fried, and G. Jalsovszky, Thin Solid Films, **388**, 295 (2001).

63. Y. Y. Song, Z. D. Gao, J. J. Kelly, and X. H. Xia, Electrochem. Solid State Lett., **8**, C148 (2005).
64. C.-H. Wang, Y.-Y. Song, J.-W. Zhao, and X.-H. Xia, Surf. Sci., **600**, L38–L42 (2006).
65. E. S. Kooij, R. W. Despo, F. P. J. Mulders, and J. J. Kelly, J. Electroanal. Chem., **406**, 139 (1996).
66. E. S. Kooij, R. W. Despo, and J. J. Kelly, Appl. Phys. Lett., **66**, 2552 (1995).
67. M. J. Eddowes, J. Electroanal. Chem., **280**, 297 (1990).
68. E. K. Propst and P. A. Kohl, J. Electrochem. Soc., **141**, 1006 (1994).
69. E. A. Ponomarev and C. Levy-Clement, Electrochem. Solid State Lett., **1**, 42 (1998).
70. R. B. Wehrspohn, J. N. Chazalviel, F. Ozanam, and I. Solomon, Thin Solid Films, **297**, 5 (1997).
71. R. B. Wehrspohn, J. N. Chazalviel, and F. Ozanam, J. Electrochem. Soc., **145**, 2958 (1998).
72. V. Lehmann and S. Ronnebeck, J. Electrochem. Soc., **146**, 2968 (1999).
73. K. J. Chao, S. C. Kao, C. M. Yang, M. S. Hseu, and T. G. Tsai, Electrochem. Solid State Lett., **3**, 489 (2000).
74. R. B. Wehrspohn, F. Ozanam, and J. N. Chazalviel, J. Electrochem. Soc., **146**, 3309 (1999).
75. A. Bsiesy, F. Gaspard, R. Herino, M. Ligeon, F. Muller, and J. C. Oberlin, J. Electrochem. Soc., **138**, 3450 (1991).
76. M. Ligeon, F. Muller, R. Herino, F. Gaspard, J. C. Vial, R. Romestain, S. Billat, and A. Bsiesy, J. Appl. Phys., **74**, 1265 (1993).
77. S. Billat, F. Gaspard, R. Herino, M. Ligeon, F. Muller, F. Romestain, and J. C. Vial, Thin Solid Films, **263**, 238 (1995).
78. A. Bsiesy, B. Gelloz, F. Gaspard, and F. Muller, J. Appl. Phys., **79**, 2513 (1996).
79. A. Bsiesy, F. Muller, M. Ligeon, F. Gaspard, R. Herino, R. Romestain, and J. C. Vial, Phys. Rev. Lett, **71**, 637 (1993).
80. P. M. M. C. Bressers, J. W. J. Knapen, E. A. Meulenkamp, and J. J. Kelly, Appl. Phys. Lett., **61**, 108 (1992).
81. E. A. Meulenkamp, L. M. Peter, D. J. Riley, and R. I. Wielgosz, J. Electroanal. Chem., **392**, 97 (1995).
82. L. M. Peter and R. I. Wielgosz, Appl. Phys. Lett., **69**, 806 (1996).
83. G. H. Schoenmakers, R. Waagenaar, and J. J. Kelly, J. Electrochem. Soc., **142**, L60 (1995).
84. J. J. Kelly, E. S. Kooij, and E. A. Meulenkamp, Electrochim. Acta, **45**, 561 (1999).
85. Phys. Stat. Sol., **202**, 8/9 (2005).
86. Phys. Stat. Sol., **204**, 5/6 (2007).